Magnetism and metal-insulator transition in $Fe(Sb_{1-x}Te_x)_2$

Rongwei Hu,[1,2] V. F. Mitrović,[2] and C. Petrovic[1]
[1]*Department of Condensed Matter Physics and Materials Science, Brookhaven National Laboratory, Upton, New York 11973, USA*
[2]*Department of Physics, Brown University, Providence, Rhode Island 02912, USA*

(Received 19 December 2008; revised manuscript received 13 January 2009; published 9 February 2009)

We have investigated structural, magnetic, and transport properties of $Fe(Sb_{1-x}Te_x)_2$ single crystals. Whereas metallic ground state is induced for $x=0.001$, canted antiferromagnetism is observed for $0.1 \leq x \leq 0.4$ with an intermediate ferromagnetic phase for $x=0.2$. With higher Te doping, semiconducting behavior is restored and the variable range hopping conduction mechanism dominates at low temperatures for $0.4 \leq x \leq 0.6$. We discuss our results within the framework of inverted metal to insulator in correlated electron insulators.

DOI: 10.1103/PhysRevB.79.064510 PACS number(s): 71.30.+h, 71.28.+d, 75.30.−m, 75.50.Pp

I. INTRODUCTION

The transition-metal compound $FeSb_2$ shows thermally activated paramagnetic susceptibility at high temperatures similar to FeSi.[1,2] The resistivity has a quasi-one-dimensional (1D) character along the c axis and shows metal-insulator crossover at 40 K. The full recovery of optical conductivity spectral weight did not occur just above the gap. Rather, it involves contributions of large energy states higher than 1 eV, suggesting that an ordinary semiconductor picture cannot account for the charge dynamics of $FeSb_2$.[3,4] Further interest in $FeSb_2$ revealed giant carrier mobility.[5] Much larger changes in magnetoresistance were observed in $Fe_{1-x}Co_xSb_2$ than in $Fe_{1-x}Co_xSi$.[6]

$FeSb_2$ and $FeTe_2$ are isomorphous with orthorhombic marcasite structure. $FeTe_2$ is reported to be a semiconductor with an antiferromagnetic transition at about 83 K.[7] Mössbauer measurements on Te-doped $FeSb_2$ indicate that Fe has $3d^6$ configuration in pure $FeTe_2$ and one electron is added per antimony atom to the conduction band in the $Fe(Sb_{1-x}Te_x)_2$ compounds.[8,9] It is also revealed that the Fe ion is tuned from Fe^{4+} to Fe^{2+} by addition of Te.[9] In this work we report the magnetism and electrical transport properties of $Fe(Sb_{1-x}Te_x)_2$ single crystals. A systematic study of the effects of Te doping on $FeSb_2$ is presented. We find that $FeSb_2$ evolves from a strongly correlated semiconductor into a metal for small Te concentration of $x=0.001$. With further increase in Te concentration, canted weak antiferromagnetic order is stabilized for $0.1 \leq x \leq 0.4$ with an intermediate ferromagnetic phase for $x=0.2$. At $x=0.4$ there is a structural phase transformation from orthorhombic *Pnnm* to monoclinic $P21/C$ structure, which drives the system to a semiconducting state.

II. EXPERIMENTAL METHOD

Single crystal samples were grown from a high-temperature melt.[10,11] Powder x-ray diffraction (XRD) spectra of the ground samples were taken with Cu $K\alpha$ radiation ($\lambda=1.5418$ Å) using a Rigaku Miniflex x-ray machine. The lattice parameters were obtained by fitting the XRD spectra using the RIETICA software.[12] Resistivity measurements were performed using a four-probe configuration on rectangular bars of polished single crystals along three principal crystal axes. Thin Pt wires were attached to electrical contacts made with Epotek H20E silver epoxy. Sample dimensions were measured with an optical microscope Nikon SMZ-800 with 10 μm resolution. Magnetization and resistivity measurements were carried out in a quantum design MPMS-5 and a PPMS-9 for temperatures from 1.8 to 350 K.

III. RESULTS AND DISCUSSION

Lattice parameters of doped samples from the powder x-ray diffraction spectra are shown in Fig. 1. The crystal structure changes from marcasite-type orthorhombic to arsenopyrite-type monoclinic at $x=0.4$ and restores to marcasite above $x=0.5$. Yamaguichi *et al.*[9] found that the arsenopyrite phase existed for $0.4 \leq x \leq 0.6$. The discrepancy with our result may be due to the different synthesis route used in analysis of polycrystalline material in Ref. 13. The arsenopyrite unit cell can be related to a pseudomarcasite cell (specified by $\vec{a}'$, $\vec{b}'$, $\vec{c}'$, and β') by vectorial relations: $\vec{a}'=(\vec{a}-\vec{c})/2$, $\vec{b}'=\vec{b}$, and $\vec{c}'=(\vec{a}+\vec{c})/2$.[13] The pseudomarcasite angle β' is 90.4° and 90.9° for $x=0.4$ and 0.5, respectively, slightly distorted from the orthorhombic structure. Conforming with Vegard's law, all axes and unit-cell volume are linearly dependent on Te concentration, implying that Te uniformly substitutes Sb in the whole doping range. Although the lattice parameter change for $x=0.001$ is below the reso-

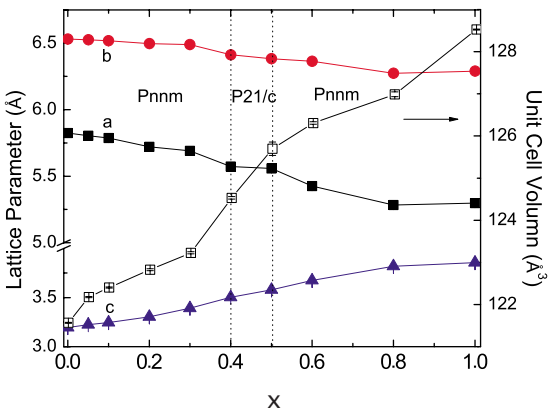

FIG. 1. (Color online) Lattice constants and unit-cell volume of $Fe(Sb_{1-x}Te_x)_2$ versus nominal Te concentration x.

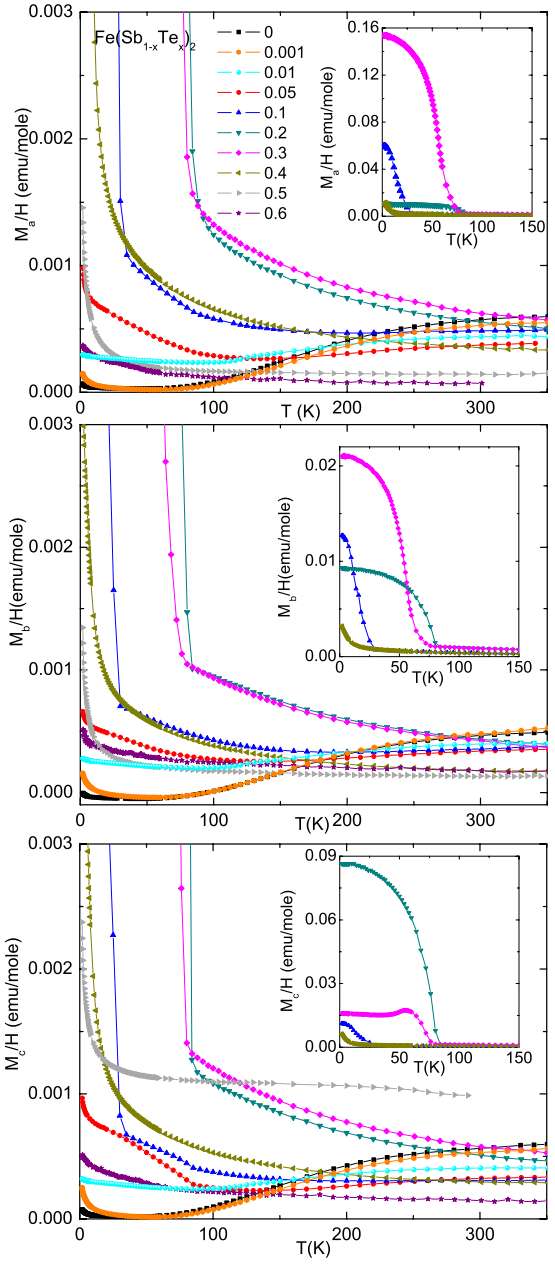

FIG. 2. (Color online) Magnetic susceptibility of $Fe(Sb_{1-x}Te_x)_2$ for $0 \leq x \leq 1$ in 1 kOe magnetic field applied parallel to three crystal axes. The insets show the low-temperature part of ferromagnetic samples for $x=0.1-0.4$.

lution of x-ray diffraction measurement, the significant change in the transport properties for $x=0.001$ indicates that band filling of $FeSb_2$ has been affected by Te doping. The increase in the magnetic-susceptibility tail at the lowest temperatures for $x=0.001$ is in line with those for higher doping (Fig. 2).

The magnetic susceptibility along the three crystal axes of $Fe(Sb_{1-x}Te_x)_2$ $(0 \leq x \leq 1)$ in temperature range from 1.8 to 350 K is shown in Fig. 2. For x ranging from 0 to 0.1, the susceptibility exhibits a thermally activated behavior evident in its increase as temperature is increased from 40 to 350 K. The thermally activated behavior can be described by the narrow-band-small-gap model:[2]

$$\chi(T) = \frac{2N\mu_B^2 p \exp(\Delta_\chi/T)[\exp(W/T)-1]}{W[1+\exp(\Delta_\chi/T)]\{1+\exp[(\Delta_\chi+W)/T]\}} + \chi_0.$$

The fit of the polycrystalline average to this model gives a spin gap of $\Delta_\chi=425$ K and rectangular bandwidth of $W=310$ K for pure $FeSb_2$.

As Te is added to a pure $FeSb_2$, the activated behavior diminishes and the Curie-Weiss term due to the Fe^{3+} moment sets in, clearly visible in Fig. 2 for $x=0.2$. This behavior can be understood in the context of Goodenough's band model for the marcasite structure.[14] According to this model $FeSb_2$ has two filled Λ bands and one empty Ξ conduction band, corresponding to the low-spin Fe^{4+} $3d^4$ configuration.[14] The added one electron per Te atom in $Fe(Sb_{1-x}Te_x)_2$ will fill the empty Ξ band and presumably induce metallicity. Indeed, we observed increasing absolute values of Pauli susceptibility χ_0 for x up to 0.3 and Curie-Weiss temperature θ_{CW} for x up to 0.2. At $x=0.2$, θ_{CW} diminishes due to contributions of ferromagnetic interactions for $x=0.2$. The parameters of the fit to the narrow-band-small-gap model and to the Curie-Weiss law are summarized in Table I. With increasing Te concentration from 0 to 0.1, the spin gap remains the same order of magnitude, ~0.04 eV, while the band is broadened by nearly two times. The high-temperature effective moment per Fe grows linearly with x, with a slope of $0.9e$/Te atom, and reaches its maximum of approximately $1.1\mu_B$/formula unit for FeSbTe. For $x>0.5$, it is predicted that the addition of an electron in the Ξ state of the low-spin configuration would contribute negatively to the effective moment.[9] Our observation confirms this prediction.

Ab initio electronic calculation indicates that $FeSb_2$ is close to magnetic instability.[3] Doping studies of $Fe_{1-x}Co_xSb_2$ and $Fe_{1-x}Cr_xSb_2$ give evidence of weak ferromagnetism and canted antiferromagnetism, and thus confirm the predictions of the *ab initio* electronic calculation. In contrast to Co and Cr dopings, Te substitution of the Sb ligand site will not introduce extrinsic magnetic moments. Therefore the low-temperature magnetic ordering seen in $Fe(Sb_{1-x}Te_x)_2$ is entirely attributed to the characteristics of the electron structure of the Fe matrix. To further test this idea, we explore low-temperature behavior of the susceptibility.

The low-temperature magnetic susceptibilities for $0.1 \leq x \leq 0.4$ is shown in the insets of Fig. 2. In 1 kOe magnetic field, samples for all four Te doping concentrations show a ferromagnetic feature for field parallel to each of three principal crystal axes. The feature saturates to a finite value and is sensitive to magnetization history below certain transition temperature, identified as T where the χ jump occurs. This is evidenced in hysteresis loops shown in Fig. 3. To better understand the nature of the ferromagnetic state, we explore the applied magnetic-field dependence of the susceptibility. The ferromagnetic tail at low temperatures evolves into a peak whose position is field dependent as illustrated in Fig. 4. This is an indication that the magnetic ordering is of canted antiferromagnetic nature as in $Fe_{1-x}Cr_xSb_2$.[15] A slight deviation from antiparallel arrangement of spins results in the spontaneous magnetization at low temperatures. The canting angle is approximately $\theta_c \approx 0.6° - 0.8°$ for $0.1 \leq x \leq 0.4$. It was calculated as $\theta_c = 2\sin^{-1}(M_s/2M_{max})$ where M_s is the saturation

TABLE I. Parameters of the fits to the polycrystalline average of M/H data and the electrical transport activation energy gap for resistivity above 200 K.

x	Δ_χ (K)	W (K)	χ_0 (emu/mol)	μ_{eff} (μ_B)	Θ_{CW} (K)	T_C (K)	M_s ($10^{-3}\mu_B$)	Δ_ρ (K)
0	425	310	4×10^{-6}					225
0.001	419	352	9×10^{-6}					124
0.01	336	451	1.8×10^{-4}	0.25	−133			36
0.05	453	660	2.1×10^{-4}	0.33	−195			44
0.1	568	710	3.6×10^{-4}	0.44	−420	12	5.8	126
0.2			6.0×10^{-4}	0.60	−21	77	6.0	135
0.3			8.0×10^{-4}	0.74	−74	61	10.5	143
0.4			1.5×10^{-4}	0.97	−127	5		177
0.5			1.1×10^{-4}	1.10	−791			352
0.6			5×10^{-5}	0.88	−338			907

moment and M_{max} is the magnetic moment of the Fe ion which is estimated from the high-temperature effective moment. This is consistent with the negative Curie-Weiss temperatures θ_{CW} which also testify that the underlying magnetic coupling is antiferromagnetic. However, the ferromagnetic tail for $T<40$ K for $x=0.2$ remains unchanged in different magnetic fields. Therefore an intermediate ferromagnetic phase may exist for $x=0.2$. The biased hysteresis loops observed in Figs. 3(c) and 3(d) indicate complex magnetic structure brought about by the coupling of antiferromagnetic and ferromagnetic domains. Competing antiferromagnetic and ferromagnetic coupling may also be the cause of nonmonotonic evolution of θ_{CW} with Te substitution. Biased loops for $x=0.2$ are temperature dependent as seen in Fig. 3(d). Above $x=0.6$, no magnetic ordering was observed down to 1.8 K. This is in agreement with the Mössbauer measurement by Sharma and Wagner[8] but contrary to reports that $FeTe_2$ orders antiferromagnetically at 83 K.[7,8]

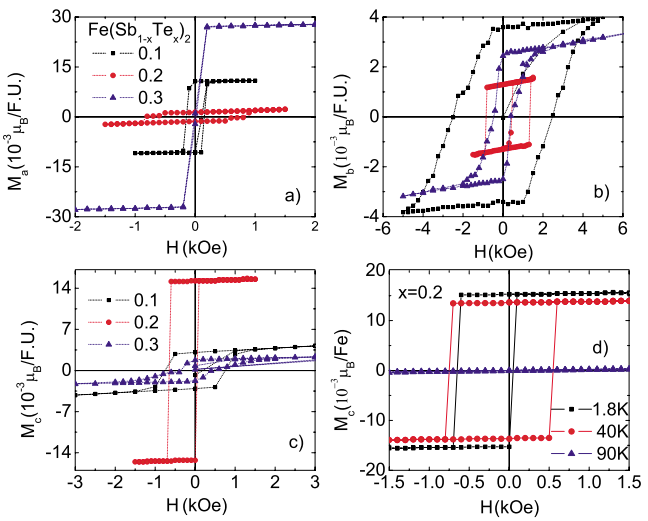

FIG. 3. (Color online) (a)–(c) Hysteresis loops of $Fe(Sb_{1-x}Te_x)_2$ for $0.1\leq x\leq 0.3$ at 1.8 K. (d) At temperature above magnetic transition, the hysteresis loop disappears; for example $x=0.2$, no hysteresis is observed at $T=90$ K.

We proceed to the analysis of the resistivity data. The temperature dependence of resistivity along all crystal axes is plotted in Figs. 5(a)–5(c). The metallic ground state is induced for all crystalline axis for temperatures below 8 K for $x=0.001$ and below 200 K for $0.01\leq x\leq 0.2$. The metallic temperature regime increases with Te doping. Above 200 K, the metallic resistivity gives way to semiconducting behavior. Lowest residual resistivities are observed for Te concentration of $x=0.001$ in close proximity to the strongly correlated insulating state of $FeSb_2$ for current applied along the highly conducting c axis. A similar effect was observed in Co-doped FeSi, where a small concentration of Co (~0.01) induces a metallic and magnetic state.[16] For higher concentration $0.3\leq x$, there is an increase in resistivity and the semiconducting behavior extends to the whole temperature range.

For $0.4\leq x\leq 0.6$, in the middle of the alloy series, the polycrystal average resistivities are plotted as a function of

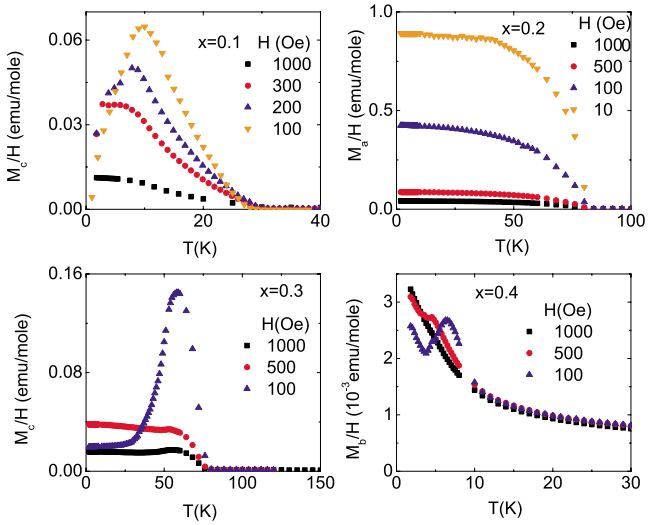

FIG. 4. (Color online) Temperature dependence of magnetic susceptibility, in the low-temperature region, at different applied fields and Te concentrations ranging from 0.1 to 0.4. These plots clearly show magnetic-field dependence of the canted antiferromagnetic transition for $0.1\geq x\leq 0.4$.

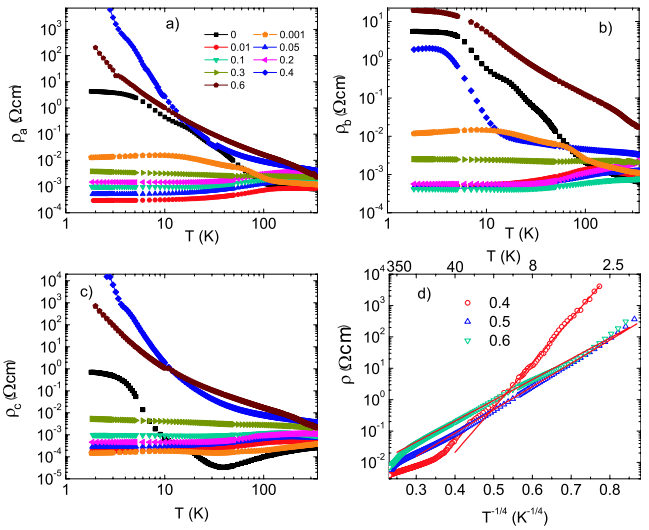

FIG. 5. (Color online) (a)–(c) Temperature dependence of resistivity for current applied along three crystal axes for $0 \leq x \leq 0.6$. Low-temperature polycrystal average resistivities for $x=0.01$ and 0.05 are plotted as a function of T^2 in inset. (d) Polycrystal average resistivity for $x=0.4-0.6$ versus $T^{-1/4}$ on a semilog scale. The straight line is the fit to $\rho=\rho_0 \exp(T_0/T)^{1/4}$.

$T^{-1/4}$ on a semilog scale in Fig. 5(d). The linear fits to the data, i.e., $\rho=\rho_0 \exp(T_0/T)^{1/4}$, reveals that the variable range hopping (VRH) mechanism dominates the electrical conduction at low temperatures for heavily disordered alloys in the Te concentration range of $0.4 \leq x \leq 0.6$. In the VRH model (Table II), conduction is due to the hopping of carriers between localized states, which are separated by R in space and by W in energy. The wave functions of localized states decay within a localization length ξ. The characteristic temperature T_0 is related to localization length ξ and density of states at the Fermi surface by $k_B T_0 = 21/N(E_F)\xi^3$.[17] The density of states, $N(E_F)$, is estimated by the Sommerfeld coefficient γ from the heat-capacity measurements,[18] i.e., $N(E_F) = 3\gamma/\pi^2 k_B^2$. The calculated localization length, being of the same order as the lattice constant, indicates that the localized state is restricted within the unit cell of $FeSb_2$. It increases with increasing Te concentration. This implies that the system is more disordered at the border line of structural transformation in Sb rich end. Hopping range R and hopping energy W are estimated by equations: $R=[3\xi/2\pi N(E_F)k_B T]^{1/4}$ and $W=3/4\pi R^3 N(E_F)$. Conditions $R > \xi$ and $W \gg k_B T$ are satisfied in the VRH region so that hopping sites are spatially separated and carriers are localized in potentials larger than thermal fluctuations. With increasing x, localized states are positioned further apart and carriers acquire less energy for transition.

TABLE II. Parameters of variable range hopping (R and W are estimated for $T=5$ K, deep in the VRH region)

x	T_0 (K)	ξ (Å)	R (Å)	W (K)
0.4	114 220	1.9	15.8	21
0.5	84 753	4.5	19.9	11
0.6	54 014	6.1	24.0	10

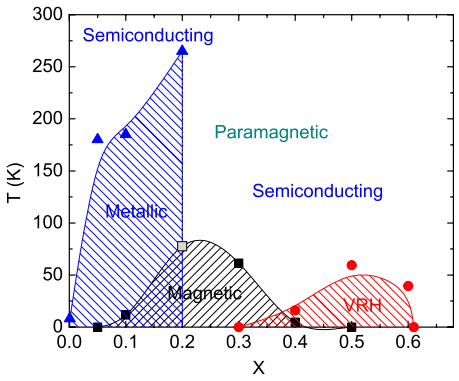

FIG. 6. (Color online) Phase diagram of $Fe(Sb_{1-x}Te_x)_2$. Black squares are the antiferromagnetic transition temperature, derived from the steepest slope of the magnetic-susceptibility curve. Gray square is the transition temperature of the ferromagnetic phase at $x=0.2$. Red circles are the high-temperature limits for VRH fits in Fig. 5. Blue triangles are the turning points at which temperature coefficient of resistivity changes sign.

From the data presented here, we compiled a combined magnetic and electronic transport phase diagram shown in Fig. 6. Whereas the metallic state is induced with very small Te concentration of $x=0.001$, the magnetic ground state emerges at $x=0.1$ and vanishes for $x=0.4$ when the structural changes to monoclinic $P21/c$ occur. The highest ordering temperature of $T_C=77$ K in the alloy series is observed in $FeSb_{1.6}Te_{0.4}$. With further addition of Te the ground state becomes semiconducting and T_C diminishes.

Within the LDA+U framework, Anisimov *et al.*[19] have shown that the ground state of FeSi is very close in energy to a ferromagnetic metallic state with a moment of $\mu \sim 1\mu_B$/Fe. Transition from nonmagnetic insulator to ferromagnetic metal in $FeSi_{1-x}Ge_x$ was well described using this approach.[20] Likewise, the *ab initio* LDA+U calculation predict a nearly ferromagnetic state in $FeSb_2$.[21] Magnetism readily appears with substitution on the Fe site (Co, Cr).[15,22,23] As opposed to FeSi, weak magnetic order ($\mu \sim 10^{-2}\mu_B$/Fe) emerges deep in the metallic state and persists through the range of heavily doped alloys. Ligand substitution with Te atoms is consistent with this picture. Transition temperatures ($T_C \sim 80$ K) are higher than in $Fe_{1-x}Co_xSb_2$ and are comparable with the $Fe_{1-x}Cr_xSb_2$ system even though we found the nonmagnetic ground state for $FeTe_2$ as opposed to $CrSb_2$. Given these facts together with the unusual overestimate of the gap by a factor of ~10, we conclude that the existing band-structure picture cannot explain properties of $FeSb_2$.[3,21]

The model of the multiband correlated electron covalent insulator (CI) based on the dynamic mean-field approach (DMFT) explains well the optical conductivity $\sigma(T,\omega)$ and magnetic susceptibility of $FeSb_2$.[24] On the other hand, this model does not capture several important observations. There is a separation of metallic and magnetic energy scales in doping on both Fe (Cr) and ligand (Te) sites. It may be explained by a smaller (indirect) energy gap responsible for transport and a larger (direct) energy gap responsible for spin

excitations.[25] This is further supported by evidence of strong electron-phonon interactions in this material.[3,26] In addition, induced magnetic order is weak, implying that magnetism is a consequence rather than a driver of metal to insulator transition. Further development of the CI model within DMFT can significantly improve a comprehensive understanding of gap formation and other interesting properties of all correlated electron insulators.

IV. CONCLUSION

In conclusion, we have studied the magnetic and electrical transport properties of $Fe(Sb_{1-x}Te_x)_2$. The metallic state and magnetism are induced for $0.001 \leq x \leq 0.2$ and $0.1 \leq x \leq 0.5$, forming a rich phase diagram. In the heavily doped regime, the system reenters the semiconducting state and VRH conduction dominates at low temperatures. Our results show that properties of $FeSb_2$ defy complete description based on either LDA+U or DMFT theoretical methods.

ACKNOWLEDGMENTS

This work was carried out at the Brookhaven National Laboratory, which is operated for the U.S. Department of Energy by Brookhaven Science Associates (Contract No. DE-Ac02-98CH10886). This work was supported by the Office of Basic Energy Sciences of the U.S. Department of Energy.

[1] C. Petrovic, J. W. Kim, S. L. Bud'ko, A. I. Goldman, P. C. Canfield, W. Choe, and G. J. Miller, Phys. Rev. B **67**, 155205 (2003).
[2] C. Petrovic, Y. Lee, T. Vogt, N. Dj. Lazarov, S. L. Bud'ko, and P. C. Canfield, Phys. Rev. B **72**, 045103 (2005).
[3] A. Perucchi, L. Degiorgi, R. Hu, C. Petrovic, and V. Mitrović, Eur. Phys. J. B **54**, 175 (2006).
[4] M. J. Rozenberg, G. Kotliar, and H. Kajueter, Phys. Rev. B **54**, 8452 (1996).
[5] Rongwei Hu, V. F. Mitrovic, and C. Petrovic, Appl. Phys. Lett. **92**, 182108 (2008).
[6] Rongwei Hu, K. J. Thomas, Y. Lee, T. Vogt, E. S. Choi, V. F. Mitrovic, R. P. Hermann, F. Grandjean, P. C. Canfield, J. W. Kim, A. I. Goldman, and C. Petrovic, Phys. Rev. B **77**, 085212 (2008).
[7] J. Llewellyn and T. Smith, Proc. Phys. Soc. London **29**, 203 (1959).
[8] Y. K. Sharma and F. E. Wagner, Hyperfine Interact. **59**, 341 (1990).
[9] G. Yamaguchi, M. Shimada, M. Koizumi, and F. Kanamaru, J. Solid State Chem. **34**, 241 (1980).
[10] P. C. Canfield and Z. Fisk, Philos. Mag. B **65**, 1117 (1992).
[11] Z. Fisk and J. P. Remeika, in *Handbook on the Physics and Chemistry of Rare Earths*, edited by K. A. Gschneider and J. Eyring (Elsevier, Amsterdam, 1989), Vol. 12.
[12] B. Hunter, "RIETICA—A Visual RIETVELD Program," International Union of Crystallography Commission on Powder Diffraction Newsletter No. **20** (Summer), 1998 (http://www.rietica.org).
[13] E. Bjerkelund and A. Kjekshus, Acta Chem. Scand. (1947-1973) **24**, 3317 (1970).
[14] J. B. Goodenough, J. Solid State Chem. **5**, 144 (1972).
[15] Rongwei Hu, V. F. Mitrovic, and C. Petrovic, Phys. Rev. B **76**, 115105 (2007).
[16] M. A. Chernikov, L. Degiorgi, E. Felder, S. Paschen, A. D. Bianchi, H. R. Ott, J. L. Sarrao, Z. Fisk, and D. Mandrus, Phys. Rev. B **56**, 1366 (1997).
[17] V. Ambegaokar, B. I. Halperin, and J. S. Langer, Phys. Rev. B **4**, 2612 (1971).
[18] Rongwei Hu, V. F. Mitrovic, and C. Petrovic (unpublished).
[19] V. I. Anisimov, S. Yu. Ezhov, I. S. Elfimov, I. V. Solovyev, and T. M. Rice, Phys. Rev. Lett. **76**, 1735 (1996).
[20] V. I. Anisimov, R. Hlubina, M. A. Korotin, V. V. Mazurenko, T. M. Rice, A. O. Shorikov, and M. Sigrist, Phys. Rev. Lett. **89**, 257203 (2002).
[21] A. V. Lukoyanov, V. V. Mazurenko, V. I. Anisimov, M. Sigrist, and T. M. Rice, Eur. Phys. J. B **53**, 205 (2006).
[22] Rongwei Hu, R. P. Hermann, F. Grandjean, Y. Lee, J. B. Warren, V. F. Mitrovic, and C. Petrovic, Phys. Rev. B **76**, 224422 (2007).
[23] Rongwei Hu, V. F. Mitrovic, and C. Petrovic, Phys. Rev. B **74**, 195130 (2006).
[24] J. Kuneš and V. I. Anisimov, Phys. Rev. B **78**, 033109 (2008).
[25] S. Paschen, E. Felder, M. A. Chernikov, L. Degiorgi, H. Schwer, H. R. Ott, D. P. Young, J. L. Sarrao, and Z. Fisk, Phys. Rev. B **56**, 12916 (1997).
[26] A.-M. Racu, D. Menzel, J. Schoenes, M. Marutzky, S. Johnsen, and B. B. Iversen, J. Appl. Phys. **103**, 07C912 (2008).